Oscillations in the mean transition time of a particle scattered on a double slit potential

Reuven Ianconescu[1,2] and Eli Pollak[2]

[1] *Shenkar College of Engineering and Design,*

Anna Frank St 12, Ramat Gan, Israel

[2] *Chemical and Biological Physics Department,*

Weizmann Institute of Science, 76100 Rehovoth, Israel

(Dated: December 23, 2018)

Abstract

Scattering through a double slit potential is one of the most fundamental problems in quantum mechanics. It is well understood that due to the superposition of amplitudes one observes a spatial interference pattern in the scattered wavefunction reflecting the superposition of amplitudes coming from both slits. However, the effect of the double slit on the mean time it takes to traverse the slit has not been considered previously. Using a transition path time formalism we show that when a single Gaussian wavepacket is scattered through a double slit potential, one finds not only oscillations in the scattered density resulting from the spatial interference created by the splitting of the wavepacket but also an oscillatory pattern in the mean scattering time. Long times are associated with low values of a suitably defined momentum, short times with higher values. The double slit thus serves as a momentum filtering device. We also find an interference pattern in the time averaged momentum weak value profile of the scattered particle implying that the double slit also acts as a weak momentum filter. These results not only demonstrate the value of considering transition path time distributions in their quantum mechanical context but also present a challenge to semiclassical approximations - can they also account for temporal interference?

I. INTRODUCTION

The diffraction of material particles scattered through a double slit potential or a grating is well documented. For example, Nairz et al [1], using a time of flight experimental setup, measured the diffraction pattern of suitably prepared Fullerene molecules scattered through a grating. The process is well understood and a brief history of the milestones in its discovery and experimental verification for a variety of physical systems may be found in Refs. [1, 2]. Underlying it all is the wave description of matter and the superposition principle. The superposition of two waves coming from each of the two slits creates a spatial diffraction pattern with maxima and minima corresponding to constructive and destructive interference of the two components.

Diffraction in time is also a well known phenomenon, especially in the context of time dependent perturbations of the system under study. Moshinsky [3] considered "Diffraction in time" showing that one may observe transient in time oscillations of the flux associated with scattering through a shutter that is opened at say $t = 0$. Experiments have demonstrated how time dependent modulations [4, 5] or initial temporal separation of beams [6] lead to temporal diffraction patterns. The common theme that characterizes these studies [7] is that the interference in time pattern is created either by a time dependent modulation, that is the Hamiltonian describing the system is time dependent, or by an initial preparation of wavepackets that are separated in time.

A simple model of the two slit spatial interference phenomenon may be found for example in Ref. [8]. Two Gaussians originate at two different points and are then propagated as free motion. They interfere spatially giving rise to the two slit spatial interference pattern. The same authors also consider two Gaussians originating at the same point but at different times which then proceed to interfere. Such interference in time processes have also been considered previously by Nairz et al [1]. The spatiotemporal evolution of two counter-propagating wavepackets in a suitably vibrationally excited iodine molecule have also been reported [9].

Another aspect of diffraction in time is associated with transient time observations. In such cases the Hamiltonian may be stationary. One scatters particles through a grating and measures the time of flight distribution of the particles as they hit a screen. An example of such an observation is given in Ref. [10] where the authors observe oscillations in the

arrival time at a fixed point on the screen. We will refer to such measurements as transient measurements. They reflect the time dependent density of the wavepacket as the particle hits the "screen". However, if one considers the mean time of arrival at the screen it is not clear from such measurements that it too will display oscillatory characteristics with respect to the location on the screen.

To the best of our knowledge no one has yet undertaken a study of how interference affects the mean transition time of a suitably post-selected particle. In the context of scattering through a double slit potential considered in this paper, our interest is in the mean time it takes the scattered particle to reach a point on a screen positioned either in the reflected or the transmitted region. Perhaps the reason underlying this lacuna is the fact that for many years time has been an enigma in quantum mechanics. Pauli [11] noted early on that one cannot simply define a time operator conjugate to the energy operator with commutator $i\hbar$ since this would imply an energy spectrum that goes from $-\infty$ to ∞. Hilgevoord [12] pointed out that time and space play fundamentally different roles in quantum mechanics. In a later paper [13] Hilgevoord summarized the problematics involved in defining a time operator in quantum mechanics. He traces the genesis of the problem in the work of six of the founding fathers of modern quantum theory: Dirac, Heisenberg, Bohr, Schrödinger, von Neumann and Pauli, covering the period 1925-1933. The more modern history of the evolution of defining time operators in quantum mechanics may be found in two volumes edited by Muga and coworkers, devoted to the quantum time problem [14, 15]. From these works and more recent ones [16–21], it is evident that the operator approach has not yet been resolved.

Classical mechanical transition path time distributions have been studied rather intensively in the past few years especially in the context of the folding and unfolding of proteins. In their classic experiment, Neupane et al [22, 23] measured transition times for moving from the folded to the unfolded and vice versa states of DNA hairpins. The experiments were subsequently extended [24] to measure a local velocity along the transition path. The experimental work was followed and sometimes anticipated by intensive theoretical activity [25–37]. We have more recently introduced the transition path time distribution formalism within a quantum mechanical context [38–40] which is intimately related to the presence time distribution approach [41, 42] to time in quantum mechanics. A central advantage of this formalism in the quantum mechanical context is that now time is not an operator but

a parameter in the Schrödinger equation. In contrast to the previous studies of temporal interference discussed above, it is this approach which allows us to estimate mean times and consider their interference patterns. This, for example, has enabled us recently to expose quantum coherence times in the reflection of above barrier wavefunctions [43].

There is an additional aspect of the study of the temporal time interference pattern. Semiclassical approximations have been used extensively to analyse and understand quantum effects in molecular dynamics [44]. One of the central successes of semiclassical theory has been its ability to account at least qualitatively and often quantitatively for quantum interference effects. The scattering of a material particle through a double slit potential is a classic example for the success of semiclassics in obtaining the spatial diffraction pattern [45]. The work reported here can serve as a benchmark for the study of temporal diffraction within the semiclassical approximation.

To obtain a clear picture of the quantum temporal diffraction pattern of the mean transition time we compare the mean time obtained through numerically exact quantum mechanical propagation which involves the propagation of amplitudes, with a suitably defined classical like propagation which involves the propagation of density only. A suitable tool for this purpose is the classical Wigner approximation [46], also referred to as the Wigner phase space method [47]. The initial wavepacket is represented in phase space through its Wigner transform. Since the initial state is a single Gaussian its Wigner representation is positive. It is then propagated using classical mechanics. By comparing the mean transition path time obtained from the numerically exact time evolved Gaussian wavefunction with its classical Wigner approximation, we identify the oscillatory quantum structure for the mean time it takes the particle to arrive at a point on a screen as resulting from quantum interference.

Although the oscillatory pattern observed in the mean transition time is we believe of interest on its own, it also has some remarkable consequences. As considered elsewhere [38, 48, 49], the mean time of arrival at a point on the "screen" may be used to "measure" a *mean time velocity* by considering the difference in the mean time it takes the particle to reach two adjacent points. Not surprisingly, this velocity also exhibits a diffraction related pattern such that lower velocities are correlated with longer mean times and vice versa. This implies that the double slit acts as a momentum filter.

The introduction of the weak value concept [50] has contributed significantly to our un-

derstanding of the dynamics of scattering by a double slit potential. It has been established that the weak momentum value at a post-selected position is identical to the Bohmian momentum at that point [51]. Since weak values are the results of weak measurements it became possible to use weak measurements of the momentum to experimentally recreate the Bohmian trajectories underlying the two slit dynamics [52].

We have recently shown [48] that time averaging of weak values can lead to interesting results such as a time averaged weak value energy time uncertainty principle. It is therefore of interest to consider also the transition path time averaged weak momentum measured at the screen in the context of the two slit scattering problem. In this context we note that experiments are being developed to measure the weak value of the momentum for material diffraction [53]. We find that the constructive and destructive interference of the wavefunction due to the double slit potential also serves as a weak momentum filter. Furthermore, maxima (minima) in the mean time distribution correlate with minima (maxima) of the real part of the time averaged weak valued momentum.

The model system we chose to study is the one introduced previously by Miller and coworkers [45] for the purpose of demonstrating that semiclassical methods may be used to describe spatial quantum interference phenomena. This model is presented in Section II. The resulting mean transition times and their oscillatory structure are presented in Section III. The effect of interference on the mean time averaged velocity and the real part of the time averaged weak value of the momentum is presented in Section IV. We end with a discussion of these results.

II. SCATTERING ON A MODEL TWO DIMENSIONAL SLIT POTENTIAL

To study the transition path time distribution we use the well established model of Ref. [45] whereby an electron ($m = 1$ a.u.) is scattered by the two dimensional double slit potential

$$V(x,y) = \left[V_0 - \frac{m\omega^2 y^2}{2} + \frac{m^2\omega^4 y^4}{16V_0}\right]\exp(-x^2/\alpha^2) \tag{2.1}$$

with $V_0 = 8000\,cm^{-1}$, $\omega = 600\,cm^{-1}$ and $\alpha = 50$ a.u.. The potential is displayed in Figure 1. The parameters used are typical for electron molecule interactions, however their primary purpose was to create a "reasonable' potential for the motion of an electron which mimics a double slit potential but which is smooth, rather than having sharp edges, that is discon-

tinuities which make the numerical propagation of the quantum wavepacket in some sense more difficult.

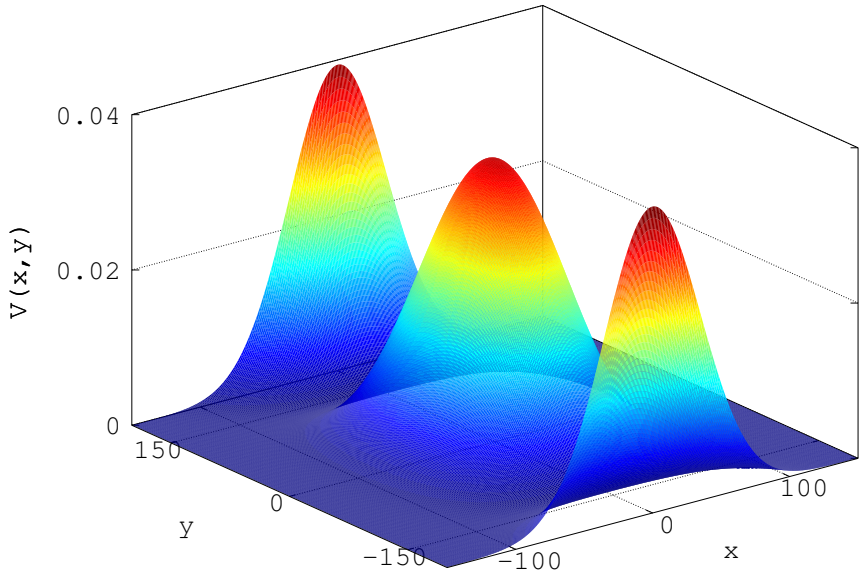

FIG. 1: The double slit potential $V(x, y)$. The potential is quartic in the y direction and Gaussian in the x direction. The axes and the potential are in atomic units.

The particle at time $t = 0$ is described by the (normalized) coherent state

$$\psi_i \equiv \psi(x, y, t = 0) = \left[\frac{\Gamma_x}{\pi}\frac{\Gamma_y}{\pi}\right]^{1/4} \exp\left[-\frac{\Gamma_x}{2}(x - x_0)^2 + \frac{i}{\hbar}p_{x0}x - \frac{\Gamma_y}{2}y^2\right] \qquad (2.2)$$

where $x_0 = -250$ a.u. is the mean position in the x direction, located at the "left" of the double slit potential. As in Ref. [45], the initial mean momentum in the x direction $p_{x0} = 0.1366$ a.u. is chosen so that the initial x kinetic energy (2048 cm^{-1}) is approximately 25% of the barrier height of the potential, located at $x = y = 0$. With this choice and the width parameters described below, we assure that motion at energies above the central barrier height and quantum tunneling effects are negligible. The major pathways for passing through the potential are the two channels, which represent the "slits" in our model.

The width parameters are chosen to be $\Gamma_x = \Gamma_y \equiv \Gamma = 25m\omega^2/(16V_0)$. With these choices the mean spatial widths in the x and y directions are $2/\sqrt{2\Gamma} = 79$ a.u.. This implies

that the spatial width of the incident wavepacket in the y direction is around 3.5 times smaller than the distance between the centers of the two slits (which is 279.34 a.u.). These conditions imply that the centers of the slits are located at an angle $\theta = \pm 0.51$ radians relative to the center of the incident wavepacket and the x axis. The initial wavepacket position and momentum in the y direction are $(0, 0)$.

The probability that the system will be at the position $\mathbf{q} = (x, y)$ at time t is

$$|\psi(\mathbf{q}, t)|^2 = \langle \psi_i | e^{i\hat{H}t/\hbar} \delta(x - \hat{x}) \delta(y - \hat{y}) e^{-i\hat{H}t/\hbar} | \psi_i \rangle \tag{2.3}$$

where $\hat{H}$ is the Hamiltonian operator ($\hat{H}(\mathbf{p}, \mathbf{q}) = \frac{\hat{\mathbf{p}}^2}{2m} + V(\hat{\mathbf{q}})$ with $\hat{\mathbf{p}} = (\hat{p}_x, \hat{p}_y)$) and the hat notation denotes operators. The transition path time probability distribution for being at the time t at the point x, y is defined to be [54]:

$$P_Q(t; x, y) = \frac{|\psi(\mathbf{q}, t)|^2}{\int_0^\infty |\psi(\mathbf{q}, t)|^2 dt}. \tag{2.4}$$

The time evolved wavefunction is obtained numerically using the split operator algorithm [55]. We use a spatial grid of 1×1 a.u. with a time step $dt = \hbar/(100V_0)$. The resulting density ($|\psi|^2$) is plotted in panel a of Figure 2 in the spatial domain $|x| \leq 1700$ and $|y| \leq 1100$, at discrete space points (x_n, y_m) separated by steps $dx = dy = 1$ for the time $t_{\text{final}} = 11340$ (all magnitudes are in atomic units). The transmission probabilities are 0.057 and 0.055 for the quantum and Wigner computations (see below), respectively. To obtain the transition path time distribution it is necessary that a full passage of the wavefunction through a given location takes place. The domain we used allows us to get reliable results for the transition path distribution up to a distance of around 900 a.u. from the slits.

For comparison and to accentuate the quantum interference pattern, we also solve for the classical Wigner time dependent density using as the initial condition the Wigner quasiprobability distribution of the incident wavefunction (Eq. 2.2), defined as:

$$\begin{aligned} W(x, y, p_x, p_y) &= \frac{1}{(2\pi)^2} \iint \psi^*(x + \hbar a/2, y + \hbar b/2) \psi(x - \hbar a/2, y - \hbar b/2) e^{i(a p_x + b p_y)} \, da \, db \\ &= \frac{1}{(\pi\hbar)^2} \exp\left[-\Gamma_x (x - x_0)^2 - \Gamma_y y^2 - \frac{(p_x - p_{x0})^2}{\hbar^2 \Gamma_x} - \frac{p_y^2}{\hbar^2 \Gamma_y} \right]. \end{aligned} \tag{2.5}$$

The Wigner dynamics time dependent density is obtained by propagating the coordinates x, y to time t using classical mechanics and the classical Hamiltonian with the two slit potential of Eq. 2.1. The classical equations of motion are solved numerically using a 4th

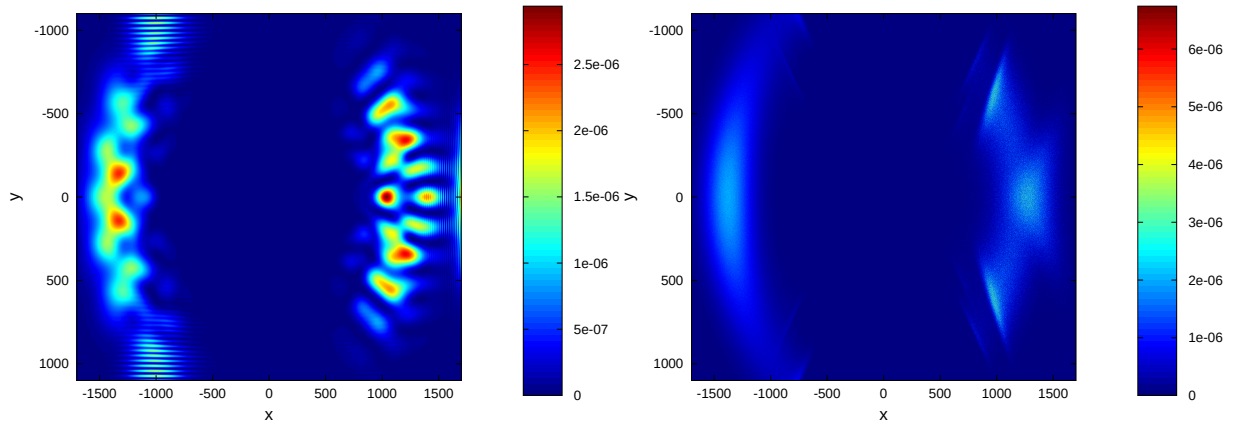

FIG. 2: The quantum (left panel) and classical Wigner dynamics (right panel) pattern obtained for the density $|\psi(x, y, t = 11340)|^2$ in the domain $|x| \leq 1700$ and $|y| \leq 1100$. The distributions are normalized to unity so that the color code reflects the probability to find the particle in a box whose size is the grid size is $dx = dy = 1$. All quantities are in atomic units. Because reflection is more probable than transmission, the density of the transmitted part ($x > 0$) has been multiplied by 15. Note the extensive interference pattern found for the quantum results which is absent in the classical Wigner density.

order Runge-Kutta integrator and a Monte Carlo sampling of the initial density. For the classical Wigner dynamics it is sufficient to use a time step which is a factor of 20 larger than that used for the quantum solution. The sample size is $2 \cdot 10^7$ trajectories. The results are histogrammed such that each destination point x, y is attributed to a box $x_n < x \leq x_n + dx$ and $y_m < y \leq y_m + dy$ with $dx = dy = 1$ a.u. .

The resulting density is compared with the quantum density in panel b of Figure 2. One notes that the classical Wigner density has two maxima in the transmitted portion corresponding to trajectories transmitted through the upper or lower slit and an additional maximum for those trajectories that are reflected off the outer barriers in each of the channels so that they come out at the center. This center peak disappears if one considers much longer scattering times. The reflected part has a single broad maximum corresponding to the trajectories reflected from the middle wall of the potential separating the two slits. The interference pattern seen in the quantum density has vanished, as expected, in this classical limit whereby the quantum density is propagated in time so that there are no interference

phenomena.

To further accentuate these differences, we plot in Fig. 3 the angular dependence of the (normalised) density distribution function $|\Psi(\theta; r, t)|^2$ at a fixed value of the radius $r = 1300$ a.u.. Panels a and b show the quantum and classical Wigner transmitted distributions (multiplied by a factor 15) panels c and d show the same for the reflected. Note the extensive quantum oscillations which are absent from the classical Wigner results.

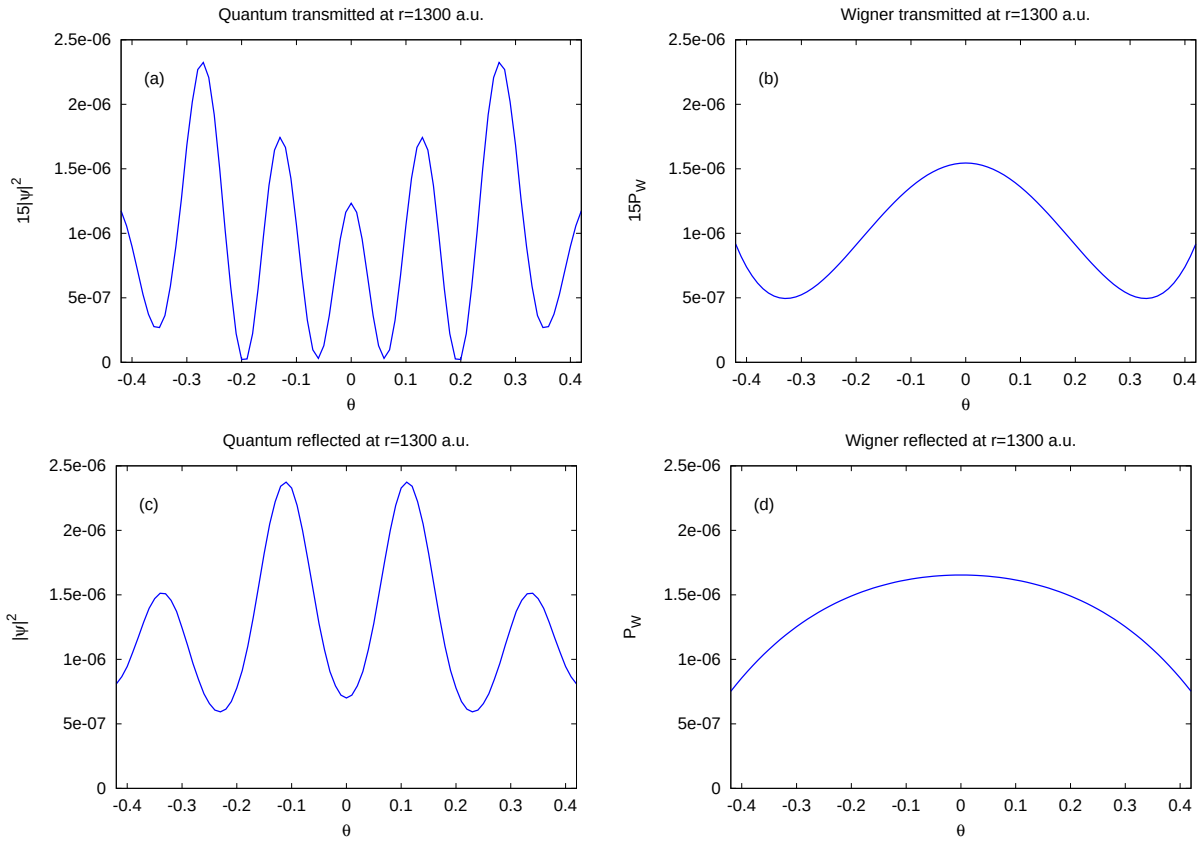

FIG. 3: Angular dependence of the probability density distribution at a fixed radius ($r = 1300$ a.u.) and a fixed time $t = 11340$ a.u.. Panels a and c show the numerically exact quantum transmitted and reflected distribution $|\Psi(\theta; r, t)|^2$, panels b and d show the results obtained using classical Wigner dynamics, $P_W(\theta; r, t)$.

III. TEMPORAL OSCILLATIONS FOR QUANTUM SCATTERING THROUGH A DOUBLE SLIT POTENTIAL

As already mentioned in the Introduction, our interest is to understand whether and how much the quantum interference affects the mean time it takes the particle to reach the screen. Even though the transient time may be oscillatory, as measured for example in Ref. [10], it is not clear that this manifests itself in the mean transition time which is a much more averaged quantity. The n-th time moment of the transition path time distribution at the point x, y is by definition

$$\langle t^n(x,y)\rangle = \int_0^\infty dt\, t^n P(t;x,y). \tag{3.1}$$

and we are especially interested in the mean ($n = 1$). The moments and distribution may also be expressed using the polar coordinates: $r = \sqrt{x^2+y^2}$ and $\theta = \tan^{-1}(y/x)$.

We note that the transition path time distribution is normalized by $N(\mathbf{q}) \equiv \int_0^\infty |\psi(\mathbf{q},t)|^2 dt$ (see Eq. (2.4)) and equivalently for the classical Wigner dynamics. Hence, for the results to be meaningful, one has to avoid regions in which $N(\mathbf{q})$ is "too small". With the parameters we have used, the transmission probabilities are much smaller than the reflection probabilities (see Figure 2). Therefore we use separate criteria for the transmitted region ($x > 0$) and the reflected region ($x < 0$). In each region we consider only values of $\mathbf{q}$ satisfying $N(\mathbf{q})/\max\{N(\mathbf{q})\} > 0.001$.

The resulting mean times of the transition path time distributions are plotted in Fig. 4. Panels a and b compare the quantum (panel a) and classical Wigner (panel b) mean times for the transmitted particle to reach the "screen" located at different fixed values of the distance r as a function of the angular variable θ.

The results for different distances r are shifted by the time it would take a free particle with momentum $p_{r_0} = p_{x_0}$ to move from one radial distance to the other. Given that the incident velocity is 0.1366 a.u. this means that the different times shown in the panels are shifted by ~ 732 a.u..

In panels c and d of Figure (4) we present the mean transition times for the reflected part of the wavepacket ($x < 0$). Here too, the quantum solution displays a time interference pattern while the classical Wigner solution does not. The classical Wigner based results are more uniform than found in the transmitted case (panel b) since the main contribution

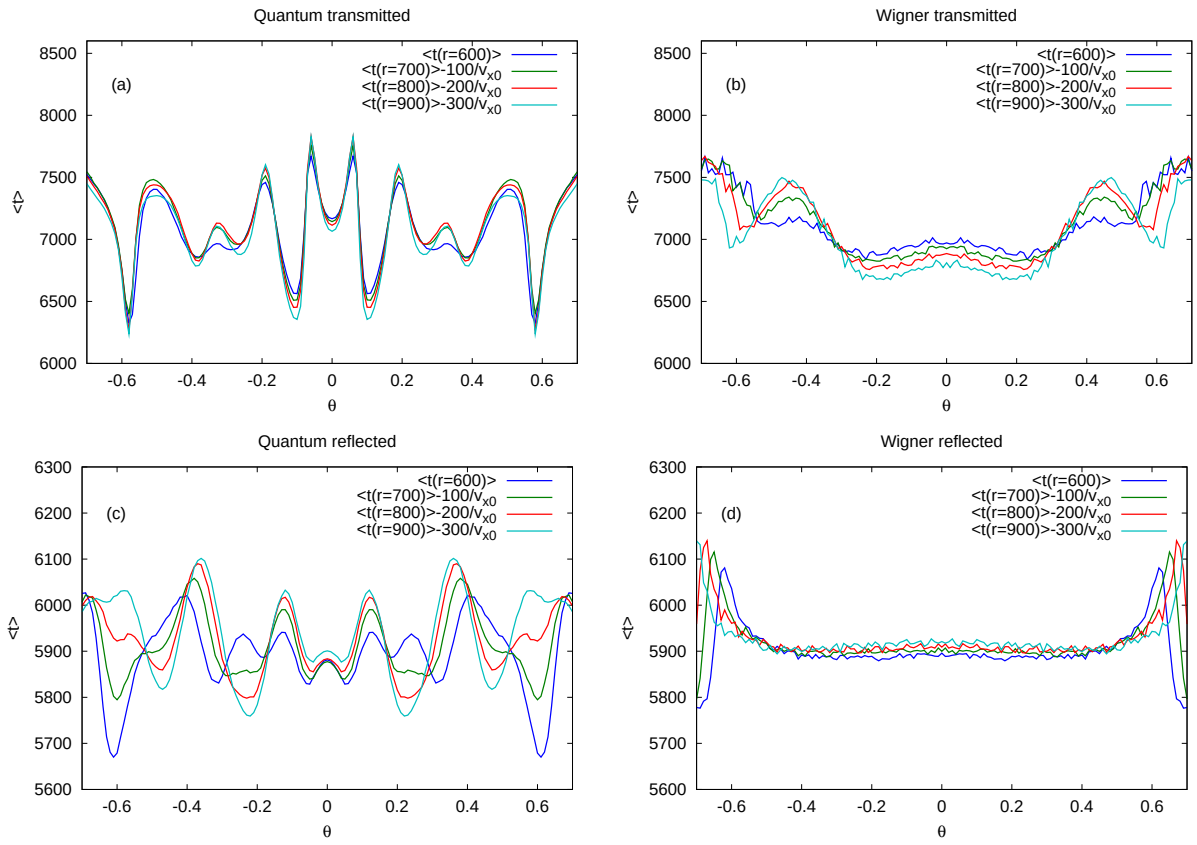

FIG. 4: Angular dependence of the mean transition path time for the transmitted and reflected scattered particles. Panels a and b show the mean transmitted times for the quantum and classical Wigner computations respectively. Panels c and d show the same for the reflected distributions. The angular dependence of the mean times at different radii are scaled by the mean time it would take a free particle at the incident mean momentum to traverse the distance between the successive points.

to the reflection comes from the repulsion by the center of the two slit potential. Since the radial distances at which we probed the mean reflection times are smaller than that of the transmitted particle, the resulting mean reflected times do not scale as nicely with the distance as in the transmitted case. For the same reason, the mean transmitted times are longer than the reflected average times by about 1200 a.u.. The transmitted times include travel from the initial center of the wavepacket to the slits (in a low potential), of approximate length $\sqrt{250^2 + (279.34/2)^2}$ a.u., while the reflected are dominated by the path to the barrier at $x = 0$ and back.

The results shown in Figure (4) are central to this paper. They show that the mean quantum time oscillates as a function of the angle while the classical Wigner mean time does not. This is found for both the transmitted and the reflected particles. As noted above, the slit angle relative to the initial center of the wavepacket is ± 0.51 radians. In the transmitted case, the classical Wigner times maximize in the vicinity of these angles. The quantum times are relatively indifferent to the angles of the slits and if anything, seem to minimize in the vicinity of the slit angles.

Both mean transmission and reflection times scale roughly with the incident momentum and this allows us to present the mean times on a single scale. However, the mean times do change as a function not only of the angle but also the radial distance. This change is more noticeable in the reflection times but is found also in the transmission times. Although the radial distances considered are such that the potential is negligible, the time diffraction pattern does not scale perfectly with the incident average momentum. This is a reflection of the fact, that as we shall see, the magnitude of the momentum distribution also oscillates roughly about the incident momentum. It is this oscillation which shows up as a more minor fluctuation of the mean time as compared to that expected for motion at the constant incident average velocity of the wavepacket.

Comparing the quantum reflection times with the classical Wigner reflection times, we note that for the reflected particles, the mean time obtained from the classical Wigner computation is almost constant in the paraxial region of small θ, showing later average arrival times associated with trajectories reflected at larger angles. The quantum mean reflection times oscillate and do not show the same structure. Furthermore, the mean time variations in the quantum reflected case are more sensitive to the radial distance than in the transmitted case as may be seen from a comparison of panels a and c of the Figure. This is partially due to the fact that the distance of the "screen" from the initial center of the incident wavepacket is smaller than in the transmitted case so that the diffraction patterns are not yet really in the "far field" region of the scattering.

IV. INTERFERENCE PATTERN FOR THE RADIAL MOMENTUM

A. Mean velocity diffraction pattern

Since we are dealing with the scattering of an electron whose atomic mass is unity, in the following we will consider interchangeably the momentum and the velocity - their numerical value in atomic units is the same. From the mean time it takes to reach a radial distance r one may infer a mean velocity by considering the difference in the mean time it takes the particle to reach two adjacent radial distances [48]:

$$v_r = \frac{\Delta r}{\langle t(r+\Delta r/2,\theta)\rangle - \langle t(r-\Delta r/2,\theta)\rangle} \equiv \frac{\Delta r}{\langle \Delta t\rangle}, \tag{4.1}$$

We will refer to this method of determination of the radial velocity as the mean time method. In practice we used $\Delta r = 0.1r$, which is a compromise: it is not too small to prevent the computation from being too sensitive to numerical noise, yet it is small enough to represent a local velocity.

In Figure 5 we display the mean time radial velocity for different radii in the transmitted region $x > 0$ for the quantum and classical Wigner solutions, calculated according to Eq. (4.1). As noted from the Figure, the quantum mean time radial velocities are almost independent of the radial distance from the origin, except at rather large deflection angles, where the probability density is in any case rather small. Comparing the mean transmission times shown in panel a of Figure 4 with the mean time velocities presented in panel a of Figure 5, we find that the minima in the plot of the mean time $\langle t(r,\theta)\rangle$ as a function of the angle θ correspond to the maxima in the mean time velocities. The same is found for the classical Wigner results: in the paraxial region the velocity is maximal, corresponding to the shorter arrival time in this region. It becomes clear that the two slit potential serves as an angular filter for the (mean time) velocity distribution of the incident particle.

The angular dependence of the reflected ($x < 0$) mean time velocities is shown in Figure 6 for different values of the radial distance. We remark that the θ dependent fluctuations diminish with the increase in the distance r. The same phenomenon occurs in the case of the classical Wigner computation: the reflected velocities are almost independent of the angle, so the reflection is almost exclusively radial. Here, the classical Wigner results are much less noisy, due to the fact that the reflection probability is ~ 20 times larger than the transmission probability so that the number of trajectories sampled is larger by the same

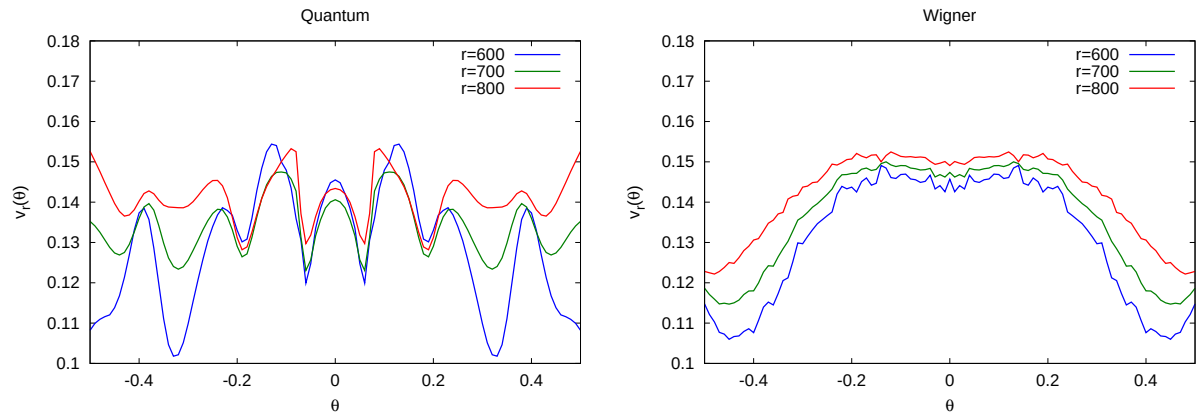

FIG. 5: Mean time radial velocities for the quantum and classical Wigner cases in the transmitted region $x > 0$ at different radii. The left panel shows the results for the quantum solution and the right panel for the classical Wigner solution. The noise in the classical Wigner solution is due to the Monte Carlo sampling of the initial points in phase space.

amount.

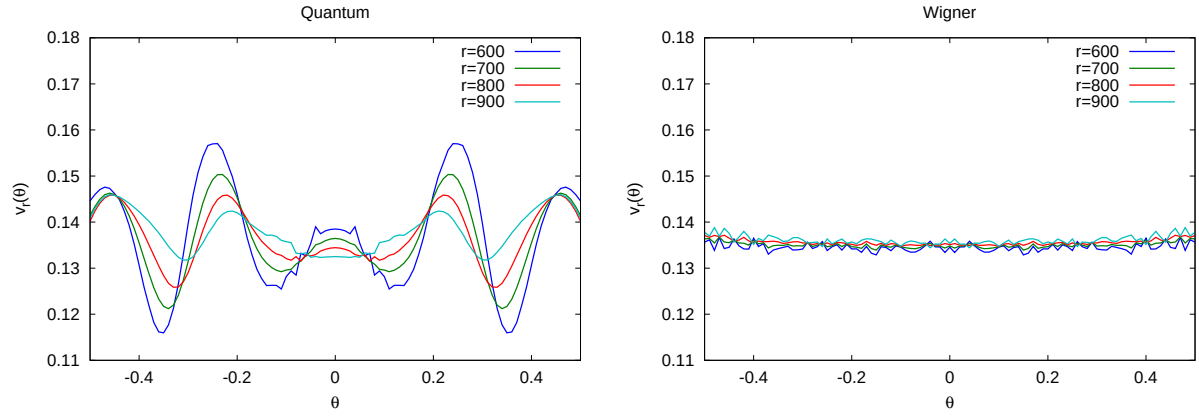

FIG. 6: Mean time radial velocities for the quantum and classical Wigner cases in the reflected region $x < 0$ at different radii. The left panel shows the results for the quantum solution and the right panel for the classical Wigner solution.

B. Diffraction of weak momentum values

Given the intense interest in the Bohmian mechanics of the two slit problem [52, 56] and the ability to measure the Bohmian trajectories experimentally [53], it is of interest to study also the weak values of the momentum in the context of their structure and how quantum diffraction affects the structure. It is also of interest since it is well known that the real part of the weak value of the momentum is identical to the Bohmian momentum [51]. Given the pre-selected wavefunction ψ, the radial weak value of the momentum at the post selected point r, θ at time t is defined as

$$p_w\left(r,\theta;t\right)=\frac{\left\langle r,\theta\left|\hat{p}_r\right|\psi_t\right\rangle}{\left\langle r,\theta|\psi_t\right\rangle}=-i\hbar\frac{\partial}{\partial r}\ln\left(\left\langle r,\theta|\psi_t\right\rangle\right). \tag{4.2}$$

The time averaged weak value of the radial momentum is by definition

$$\left\langle p_w\left(r,\theta\right)\right\rangle=\int_0^\infty dtP_Q(t;r,\theta)p_w\left(r,\theta;t\right) \tag{4.3}$$

The imaginary part of the weak momentum can be written as:

$$\mathrm{Im}\left\langle \mathrm{p_w\left(r,\theta\right)}\right\rangle=-\mathrm{i}\hbar\frac{\partial}{\partial \mathrm{r}}\int_0^\infty \mathrm{dt}\frac{\left|\left\langle \mathrm{r},\theta|\psi_\mathrm{t}\right\rangle\right|^2}{\mathrm{N(r,\theta)}}, \tag{4.4}$$

If the normalization $N(r,\theta)\equiv\int_0^\infty\left|\left\langle r,\theta|\psi_t\right\rangle\right|^2dt$ is independent of r then the imaginary part vanishes. In practice $N(r,\theta)$ depends weakly on r, so that in the regions of interest the imaginary part of the time averaged weak momentum is 2 orders of magnitudes smaller than the real part of the time averaged weak momentum and therefore we do not consider it here.

The real part of the weak value of the momentum is plotted in Figure 7. The qualitative similarity of this Figure to the results for the mean time velocity shown in the left panels of Figs. 5 and 6 is evident. One notes that the weak value oscillates as a function of the angle, having minima and maxima at the same regions as the mean time velocity. We also note that the radial weak momentum fluctuates around the average value of the incident momentum $p_{x0}=0.1366$ a.u. and is almost independent of r in the transmitted region $(x>0)$. As in the previous cases for the mean time and the mean time velocity, one notes a greater variability of the time averaged weak value momentum distribution as a function of the radial position for the reflected part, which is due to the fact that the final radial position for the reflected part is much closer to the origin of the incident wavepacket. One does note that the dependence on the radial distance diminishes as $r>700$ a.u..

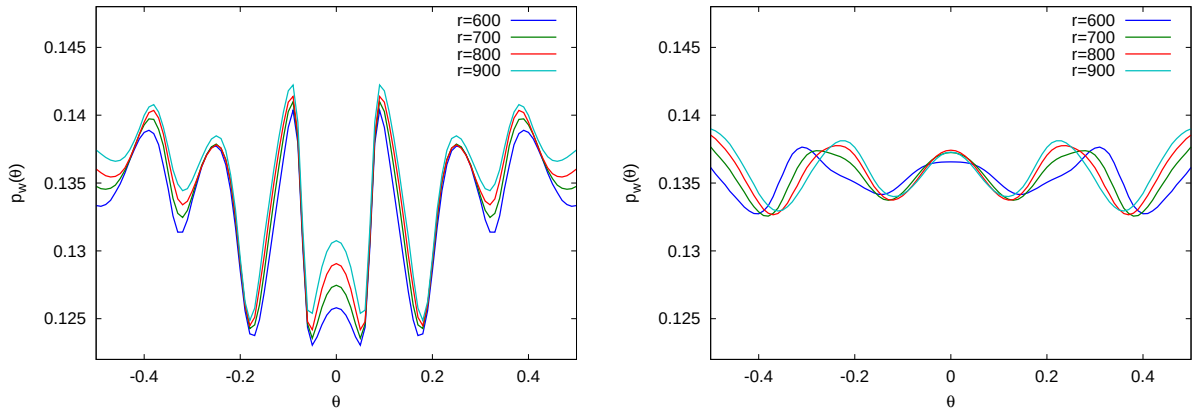

FIG. 7: Time averaged real part of the weak value of the momentum for the transmitted (left panel) and reflected (right panel) parts of the scattered wavefunction is plotted as a function of the angle at a few different values of the radial coordinate.

V. DISCUSSION

In this work we applied the quantum transition path time distribution formalism to the double slit scattering experiment. In addition to the known spatial interference pattern, we found also a temporal interference pattern for the mean transmission and reflection times. The numerically exact quantum solution for the motion of a wavepacket initiated "behind" the double slit potential and moving towards it shows minima and maxima in the mean transition time. These oscillations are absent when one replaces the quantum time evolution of the wavepacket with a classical time evolution using the classical Wigner dynamics framework. This mean temporal structure is thus a reflection of the quantum interference created by scattering through the two slits. It will be interesting to see whether the semiclassical approximation can account at least qualitatively for this phenomenon.

An oscillatory pattern is also found when considering the angular dependence of the mean time velocity of the scattered particle in both the transmitted and reflected regions. The minima and maxima in the mean time velocity distribution correlate with the maxima and minima in the mean time distribution, implying that the two slit interferometer is actually a velocity filter.

The real part of the time averaged weak momentum value was also shown to be oscillatory in its angular dependence and similar to the mean time velocity. The filtering effect thus

manifests itself also through the real part of the weak momentum values. In this context we note that at least in principle, a flux and density measurement is sufficient to establish it [57]. This means that the momentum real value distribution is accessible experimentally without need of a weak measurement apparatus.

The oscillations in the mean time and the associated velocity filtering phenomenon are due to the fact that the incident wavefunction has a breadth of momenta. The narrower the incident momentum distribution, the smaller will be the time oscillations and vice versa.

We have studied here a specific case with a specific potential. However the qualitative results should hold in general. As long as the two slits lead to a splitting of the incident wavefunction into two parts, one should expect both spatial and temporal interference. The same temporal interference should also show up in quantum diffractive scattering from a surface. As long as the spatial width of the incident wavepacket is larger than the lattice length [58], quantum interference will set in and its effect should also be observable in the time domain.

Arguably though, the most important question which should be addressed is whether the temporal oscillations can be measured experimentally. We believe that the answer is positive. From Fig. 4 one notes that the magnitude of the mean time oscillations is of order of 10% of overall time. Consider a dielectric barrier discharge source of He atoms with a velocity of 1000 m/sec and an achievable temporal width of 20 μsec [59]. The pulse is scattered on a grating with 100 nm spacing and then detected by time of flight on a screen which is a meter away from the grating. The typical time it takes to reach the screen after the scattering event would be 1 msec. A ten percent oscillation would imply a temporal resolution of 100 μsec which is a factor of five greater than the temporal width of the incident pulse. This should then be possible especially when considering recent time of flight experiments on matter wave diffraction [60].

Acknowledgments. We thank Professor Ed Narevicius for his input on the experimental feasibility of detection of the temporal interference. This work has been supported by grants from the Israel Science Foundation and the Minerva Foundation, Munich.

---

[1] O. Nairz, M. Arndt and A. Zeilinger, Am. J. Phys. **71**, 319 (2003).

[2] Y. Aharonov, E. Cohen, F. Colombo, T. Landsberger, I. Sabadini, D.C. Struppa and J.

Tollaksen, Proc. Nat. Acad. Sci. **114**, 6480 (2017).

[3] M. Moshinsky, Phys. Rev. **88**, 625 (1952).

[4] A. Steane, P. Szriftgiser, P. Desbiolles and J. Dalibard, Phys. Rev. Lett. **74**, 4972 (1995).

[5] S. Bernet, M. K. Oberthaler, R. Abfalterer, J. Schmiedmayer and A. Zeilinger, Phys. Rev. Lett. **77**, 5160 (1996).

[6] P. Szriftgiser, D. Gury-Odelin, M. Arndt and J. Dalibard, Phys. Rev. Lett. **77**, 4 (1996).

[7] L. Deng, E. W. Hagley, J. Denschlag, J. E. Simsarian, M. Edwards, C. W. Clark, K. Helmerson, S. L. Rolston and W. D. Phillips, Phys. Rev. Lett. **83**, 5407 (1999).

[8] G.G. Paulus and D. Bauer, Lect. Notes Phys. **789**, 303 (2009).

[9] H. Katsuki, H. Chiba, Ch. Meier, B. Girard, and K. Ohmori, Phys. Rev. Lett. **102**, 103602 (2009).

[10] S. Nowak, C. Kurtsiefer, T. Pfau and C. David, Opt. Lett. **22**, 1430 (1997).

[11] W. Pauli, Handbuch der Physik (Springer, Berlin, 1933), Vol. 24, pp. 83-272.

[12] J. Hilgevoord, Am. J. Phys. **70**, 301 (2002).

[13] J. Hilgevoord, Stud. Hist. Philos. Mod. Phys. **36**, 29 (2005).

[14] J. G. Muga, R. Sala Mayato, and I. L. Egusquiza, Time in Quantum Mechanics, Vol. 1, Lecture Notes in Physics Vol. 734 (Springer, Berlin, 2008).

[15] J. G. Muga, A. Ruschhaupt, and A. del Campo, Time in Quantum Mechanics Vol. 2, Lecture Notes in Physics Vol. 789 (Springer, Berlin, 2009).

[16] P. Bokes, Phys. Rev. A **83**, 032104 (2011).

[17] V. S. Olkhovsky, Phys. Usp. **54**, 829 (2011).

[18] E. E. Kolomeitsev and D. N. Voskresensky, J. Phys. G **40**, 113101 (2013).

[19] T. Pashby, Stud. Hist. Philos. Mod. Phys. **52**, 24 (2015).

[20] J. J. Halliwell, J. Evaeus, J. London, and Y. Malik, Phys. Lett. A **379**, 2445 (2015).

[21] G. Torres-Vega, J. Math. Phys. **57**, 122111 (2016).

[22] K. Neupane, D.A.N. Foster, D.R. Dee, H. Yu, F. Wang and M.T. Woodside, *Science* **352**, 239-242 (2016).

[23] K. Neupane, F. Wang, and M. T. Woodside, PNAS **114** 1329-34 (2017).

[24] K. Neupane, N. Q. Hoffer, and M. T. Woodside, Phys. Rev. Lett. **121**, 018102 (2018).

[25] G. Hummer, J. Chem. Phys. **120** 516-523 (2004).

[26] A. Berezhkovskii and A. Szabo, J. Chem. Phys. **122**, 014503(1-4) (2005).

[27] A. Berezhkovskii, A. Hummer and S. M. Bezrukov, Phys. Rev. Lett. **97**, 020601(1-4) (2006).

[28] B.W. Zhang, D. Jasnow and D.M. Zuckerman, J. Chem. Phys. **126**, 074504(1-18) (2007).

[29] A. Berezhkovskii, A. Hummer and A. Szabo, J. Chem. Phys. **130**, 205102(1-5) (2009).

[30] S.V. Malinin and V.Y. Chernyak, J. Chem. Phys. **132**, 014504(1-18) (2010).

[31] S. Chaudhury and D.E. Makarov, J. Chem. Phys. **133**, 034118(1-11) (2013).

[32] Z. Zhang and H.S. Chan, Proc. N. Acad. Sci. (USA), **109** 20919-20924 (2012).

[33] D.E. Makarov, J. Chem. Phys. **138**, 014102(1-18) (2013).

[34] H.S. Chung and V. Gopich, Phys. Chem. Chem. Phys. **16**, 18644-18657 (2014).

[35] W.K. Kim and R.R. Netz, J. Chem. Phys. **143**, 224108(1-15) (2015).

[36] R.B. Best and G. Hummer, Proc. N. Acad. Sci. (USA) **113** 3263-3268 (2016).

[37] S. V. Krivov, J. Chem. Theory Comput. **14**, 3418-3427 (2018).)

[38] E. Pollak, Phys. Rev. Lett. **118**, 070401 (2017).

[39] E. Pollak, J. Phys. Chem. Lett. **8**, 4017 (2017).

[40] E. Pollak, Phys. Rev. A **95**, 042108 (2017).

[41] J.G. Muga and C.R. Leavens, Phys. Rep. **338**, 353 (2000).

[42] K. Maji, C.K. Mondal and S.P. Bhattacharyya, Int. Rev. Phys. Chem. **26**, 647 (2007).

[43] J. Petersen and E. Pollak, J. Chem. Phys. **148**, 074111 (2018).

[44] W.H. Miller, J. Phys. Chem. A **105**, 29422955 (2001).

[45] R. Gelabert, X. Gimenez, M. Thoss, H. Wang and W. H. Miller, J. Chem. Phys. **114**(6), 2572-2579 (2001).

[46] R. Brown and E.J. Heller, J. Chem. Phys. **75** 186 (1981).

[47] R. J. Heller, J. Chem. Phys. **65**, 1289 (1976).

[48] E. Pollak and S. Miret-Artes, New J. Phys. **20**, 073016 (2018).

[49] A. M. Berezhkovskii, and D. E. Makarov, J. Chem. Phys. **148**, 201102 (2018).

[50] Y. Aharonov, D. Z. Albert, and L. Vaidman, Phys. Rev. Lett. **60**, 1351 (1988).

[51] H.M. Wiseman, New J. Phys. **9**, 165 (2007).

[52] S. Kocis, B. Braverman, S. Ravets, M.J. Stevens, R.P. Mirin, L.K. Shalm and M.A. Steinberg Science **332**, 1170 (2011).

[53] J. Morley, P.D. Edmunds and P. F. Barker, J. Phys.: Conf. Ser. **701**, 012030 (2016).

[54] J. Petersen and E. Pollak, J. Phys. Chem. Lett. **8**, 4017 (2017).

[55] R. Kosloff, J. Phys. Chem. **92**, 2087 (1988).

[56] A.S. Sanz and S. Miret-Artés, Lect. Notes Phys. **831** Chaps. 2,3 (2014).

[57] E. Cohen and E. Pollak, Phys. Rev. A, in press.

[58] J. Moix and E. Pollak, J. Chem. Phys. **134**, 011103 (2011).

[59] K. Luria, N. Lavie, and U. Even, Rev. Sci. Instr. **80**, 104102 (2009).

[60] A. R. Barnea, O. Cheshnovsky, and U. Even, Phys. Rev. A **97**, 023601 (2018).